LA-8816-MS

2

Numerical Calculation of Shock-to-Detonation from Projectile Impact

University of California

LOS ALAMOS SCIENTIFIC LABORATORY
Post Office Box 1663 Los Alamos, New Mexico 87545

Edited by

Eleanor E. Langley

UNITED STATES
DEPARTMENT OF ENERGY
CONTRACT W-7405-ENG. 36

LA-8816-MS
UC-45
Issued: April 1981

Numerical Calculation of Shock-to-Detonation from Projectile Impact

J. H. M. Fu
G. E. Cort

NUMERICAL CALCULATION OF SHOCK-TO-DETONATION FROM PROJECTILE IMPACT

by

J. H. M. Fu and G. E. Cort

ABSTRACT

This report describes the results of some numerical calculations of the impact of steel cylinders and spheres on the plastic-bonded high explosive PBX 9501. The calculations were carried out by a reactive, multicomponent, two-dimensional, Eulerian hydrodynamic computer code, 2DE. The 2DE computer code is a finite-difference code that uses the donor-acceptor-cell method to compute mixed cell fluxes.

The mechanism of shock initiation to detonation in heterogeneous explosives is best described as local decomposition at hot spots that are formed by shock interactions with density discontinuities. The liberated energy strengthens the shock so that as it interacts with additional inhomogeneities, hotter hot spots are formed, and more of the explosive is decomposed. The shock wave grows stronger until a detonation begins. This mechanism of initiation has been described numerically by the Forest Fire burn model, which gives the rate of explosive decomposition as a function of local pressure. The parameters in the Forest Fire burn model have been developed from experiments where the induced shock approximates a plane wave and are applied here to a situation where the induced shock is a divergent wave with curvature that depends on the size and shape of the projectile.

The calculated results have been compared with results from experiments involving instrumented mock and live high explosives, with projectiles of varying sizes, shapes, and velocities. We find that there is good agreement between the calculated and experimental data.

I. INTRODUCTION

A major problem in the handling and storage of munitions, and of explosive materials in general, is the possibility of the propagation of detonations from a damaged warhead or motor into nearby explosive objects. Because modern high-specific impulse solid fuels are composed mainly of explosive substances, concern with problems of sympathetic detonation has increased. This sympathetic detonation phenomenon can be caused by the blast from the primary explosion or by the impact of debris fragments. This study concentrates on impact by simulated steel debris fragments on PBX 9501: a mixture of 95% HMX-2, 2.5% nitroplasticizer, and 2.5% Estane by weight. The approach used here could be applied with more typical rocket propellants to determine critical debris particle sizes and velocities that would not cause a detonation.

The shock initiation of a detonation refers to a process in which a shock wave induced in an explosive charge develops into a propagating

detonation wave. In many experimental studies, the induced shock is generated by a plane-wave lens or by a flying plate whose characteristic length is larger than or is comparable to that of the explosive sample. In those studies, the assumption that the induced shock is a plane wave is a reasonable approximation before the arrival of the unloading rarefaction waves. The plane-wave approximation has been used in the sensitivity studies of many explosives. The well-known Pop plots for a variety of explosives are the result of those studies. The Pop plot of an explosive is a sensitivity indicator that expresses the distance of run to detonation as a function of the initial pressure.

When a small projectile strikes a high explosive (HE) sample, the propagating shock wave may decay and die, failing to initiate a detonation, or it may be amplified and initiate a detonation in the explosive. The decay of the wave is caused by rarefaction waves from interfaces and by the geometric-divergence effect; both weaken the shock. On the other hand, the propagating shock interacts with density discontinuities to create local hot spots.[1,2] The energy released from the shock-induced decomposition of the explosive at hot spots strengthens the shock. If the strengthening process prevails, a detonation will result. Thus, the shock initiation in an explosive struck by a projectile depends on the type and configuration of the target explosive and the material, velocity, and shape of the incident projectile.

II. EXPERIMENTS

The numerical study and accompanying experiments involved a single type of test. The projectiles were fired from a gas gun at a small block of PBX 9501 or 900-10 mock (1.867 g/cm^3 density) explosive. The 900-10 and some of the PBX 9501 blocks were instrumented with carbon and Manganin gauges to measure pressure and Constantan gauges to measure strains. The gauges were located on-axis at 17 mm and 34 mm from the impact surface, and 10 mm off-axis at 17 mm from the impact surface. A summary of the results that are used as a basis for comparison with the numerical calculations is given in Table I.

For 7.62-mm-diam steel cylinders striking at 845 m/s on 900-10, the peak shock pressures measured at 17 mm and 34 mm on-axis were 0.2 ± 0.03 and 0.06 ± 0.015 GPa, respectively. For the same impact on PBX 9501, the average pressures were about a factor of 8 higher because of the low-order reactions in the HE, but a full detonation did not occur. The uninstrumented PBX 9501 detonated on impact at 873 m/s with the same projectile. A cylindrical projectile almost half the diameter (3.35 mm) caused a detonation at 2178 m/s, but not at 2093 m/s.

No detonations were observed with 7.94-mm-diam spherical projectiles at velocities up to 1.85 km/s. Spherical projectiles 6.35 mm in diam did not cause detonations at velocities up to 2.506 km/s.

III. MODEL

The computation of sympathetic detonation from projectile impact was performed with the two-dimensional Eulerian reactive hydrodynamic code, 2DE (Refs. 2 and 3) using the Forest Fire burn rate.[1,2] The equation-of-state data used in these calculations are given in Appendix A. The Forest Fire burn rate parameters and Pop plot data are given in Appendix B. The Pop plots for PBX 9501 and PBX 9404* are given in Fig. 1. The density of the PBX 9501 used in these experiments and computations was 1.833 g/cm. PBX 9501 is slightly less sensitive than PBX 9404. The scatter in the experimental data for PBX 9501 gives an indication of the relative error in our calculated results. The partially reacted Hugoniots are given in Fig. 2 for 900-10, PBX 9501, and PBX 9404. Material strength was not included in the model.

The configuration of the explosive target in the computer model is cylindrical with the centerlines of the projectile and target coincident (Fig. 3). Typical mesh dimensions and numbers of computational cells are given in the r- and z- directions.

An important parameter in numerical modeling of shock waves is the artificial viscosity used in

*Composition of PBX 9404 is 94% HMX, 3% nitrocellulose, and 3% tris-β-chloroethyl phosphate.

TABLE I

SUMMARY OF EXPERIMENTAL RESULTS

I. Instrumented Targets, PBX 9501 and 900-10 (~ 1-m Range) 7.62-mm-diam x 15.24-mm-long steel cylinders at 845 ± 10 m/s.[a]

Shot No.	Target	Peak Shock Pressure (GPa)[b] On-Axis 17 mm	On-Axis 34 mm	10 mm-Off Axis 17 mm
1.	900-10	0.230	0.05	0.160
2.	900-10	0.200	0.07	0.130
3.	900-10	0.170	-	-
4.	900-10	0.140	0.07	-
5.	PBX 9501	1.250	0.41	0.900
6.	PBX 9501	1.670	-	1.550
AVG[c]	900-10	0.20 ± 0.03	0.060 ± 0.015	0.145 ± 0.02
AVG	PBX 9501	1.530 ± 0.25	0.410	1.220 ± 0.350

II. Uninstrumented Targets, PBX 9501 (~ 12-m Range)

Shot No.	Steel Projectile Size (mm Shape)	Velocity (m/s)	Result[d]
1-7	6.35-diam sphere	1238 to 2506	No go
8	7.62-diam cylinder x 15.2 long	873	Go
9	3.35-diam cylinder x 6.71 long	2275	Go
10	3.35-diam cylinder x 6.71 long	2093	No go
11	3.35-diam cylinder x 6.71 long	2178	Go
12-15	7.94-diam sphere	1700 to 1850	No go

[a]All projectiles struck the PBX 9501 surface at 0° obliquity, within 5 mm of centerline.
[b]1 GPa = 10 kbar.
[c]Excluding shot No. 4, which was farther off center than the first three.
[d]Go = detonation.

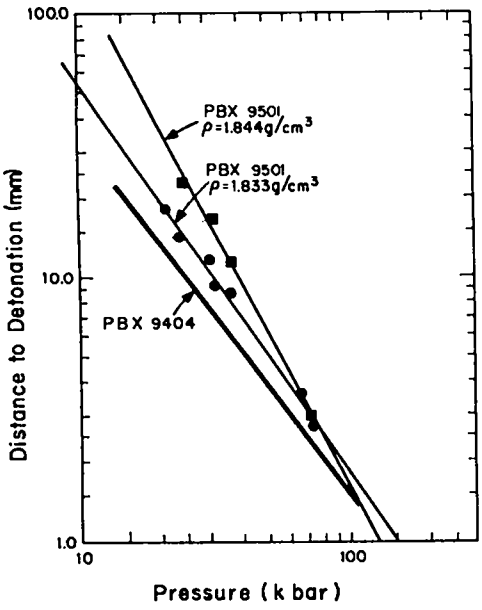

Fig. 1. Pop plots for PBX 9501 and PBX 9404.

finite-difference solutions to smear out the shock. Without artificial viscosity, the step changes in pressure and temperature across the shock can occur within a single-mesh cell and make the numerical solution unstable. There is no *a priori* method of determining the best value of the artificial viscosity for any given problem, although the shock must be smeared across a few mesh cells for stability. If the artificial viscosity is too large, the shock pressure will

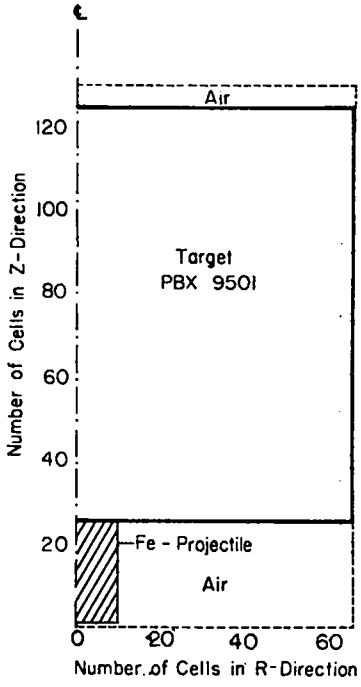

Fig. 3. Typical computer model for an impinging cylindrical projectile.

be reduced. This would be particularly serious in the present study because the Forest Fire burn rate would also be affected by the incorrect pressure. The numerical model was calibrated by ensuring that the artificial viscosity was small enough that the numerical model predicted the pressures measured in the experiments.

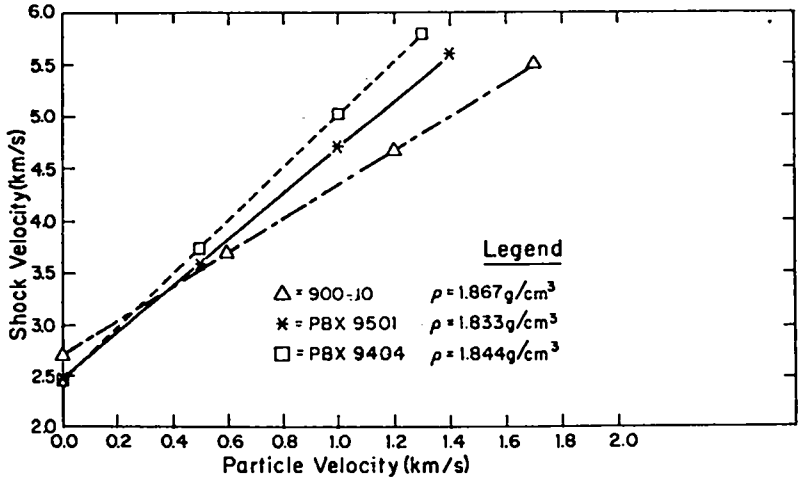

Fig. 2. Shock-particle velocity relation for 900-10, PBX 9501, and PBX 9404.

IV. RESULTS

A. 900-10

For the cylinder impact corresponding to the experimental conditions, Table II gives the calculated peak shock pressures corresponding to the measurement locations.

TABLE II

PEAK SHOCK PRESSURE IN 900-10
STRUCK BY 7.72-mm-diam CYLINDER
AT 845 m/s

Location	Peak Pressure (GPa) Measured	Calculated
On-axis, Z = 17 mm	0.200 ± 0.03	0.235
Off-axis, Z = 17 mm	0.145 ± 0.02	0.205

A series of pressure profiles (Fig. 4) taken along the axis at various times after impact shows that the leading edge of the shock wave is fairly sharp and extends across several mesh cells. The artificial viscosity used for this case is 0.25. Figure 5 shows isobars at about 2 μs after impact, indicating the curvature caused by rarefactions and divergence.

B. PBX 9501

The same calculative model was used for the PBX 9501 except for the properties. The impact velocity was again 845 m/s. Table III gives the comparison between the average experimental and calculated peak shock pressures. Although considerable decomposition of the HE took place, there was no detonation in either the experiment or the calculation. Figure 6 shows the shock pressure and the unburned mass fraction versus distance along the z-axis. The increase in peak

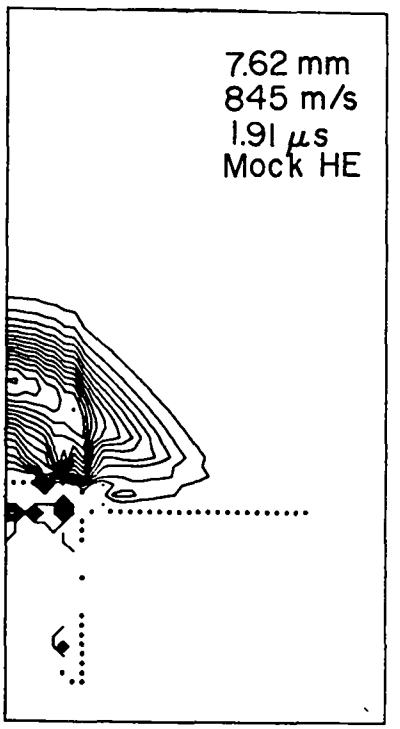

Fig. 5. Calculated isobars in 900-10 at 1.91 μs after impact by 7.62-mm-diam cylinder at 845 m/s.

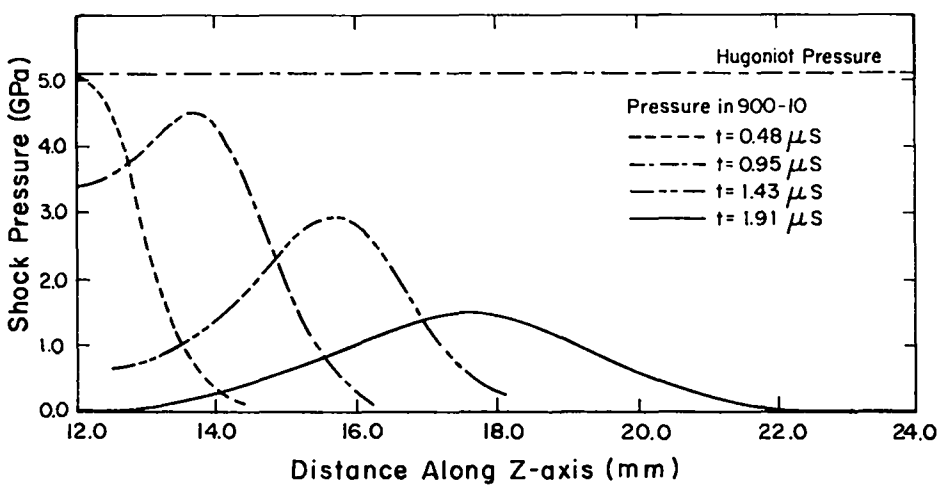

Fig. 4. Calculated pressure along centerline for 7.62-mm-diam cylinder impact on 900-10 at 845 m/s at various times after impact.

TABLE III

PEAK SHOCK PRESSURE IN PBX 9501
STRUCK BY 7.62-mm-diam CYLINDER
AT 845 m/s

Location	Peak Pressure (GPa) Measured	Calculated
On-axis, Z = 17 mm	1.530 ± 0.25	1.480
Off-axis, Z = 17 mm	1.220 ± 0.350	1.160

pressure over that observed with 900-10 is a consequence of the energy released by chemical decomposition of the PBX 9501. The curvature in the shock wave is essentially identical to that observed with 900-10 (Fig. 7).

The calculation was then repeated with identical parameters except that the cylinder velocity was increased to 873 m/s. A full detonation occurred after a run of 7.14 mm. Based on an initial pressure of 5.5 GPa from matched Hugoniots for steel and unreacted PBX 9501, the Pop plot indicates a run to detonation of 4.52 mm. The increased distance to detonation can be attributed to the decay in shock pressure with divergence. Figure 8 shows isobars and contours of constant mass fraction for times just before and just after the start of detonation, 50 computational cycles, or less than 0.5 μs apart. The corresponding

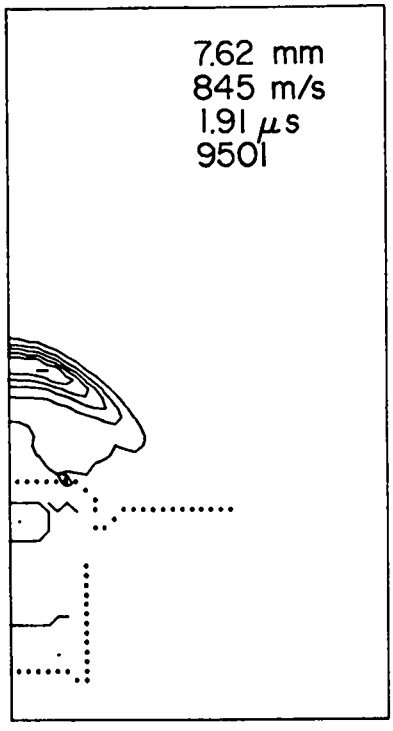

Fig. 7. Calculated isobars in PBX 9501 at 1.91 μs after impact by 7.62-mm-diam cylinder at 845 m/s.

pressure profiles and mass fractions versus distance along the centerline are shown in Fig. 9. The shock pressure is increasing with time as the

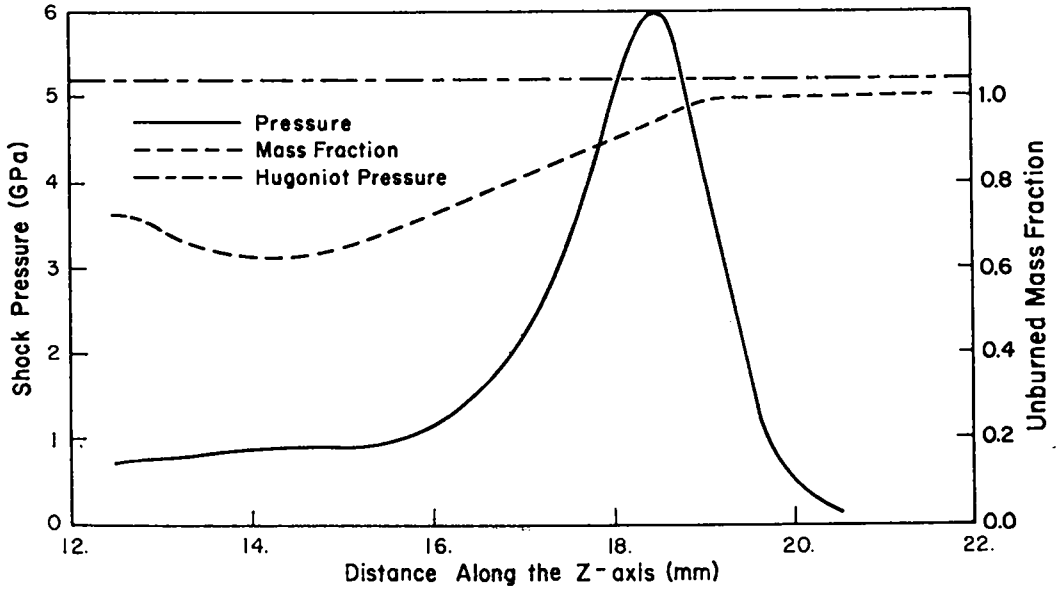

Fig. 6. Calculated pressure and unburned mass fraction for 7.62-mm-diam cylinder impact on PBX 9501 at 845 m/s, 1.91 μs after impact.

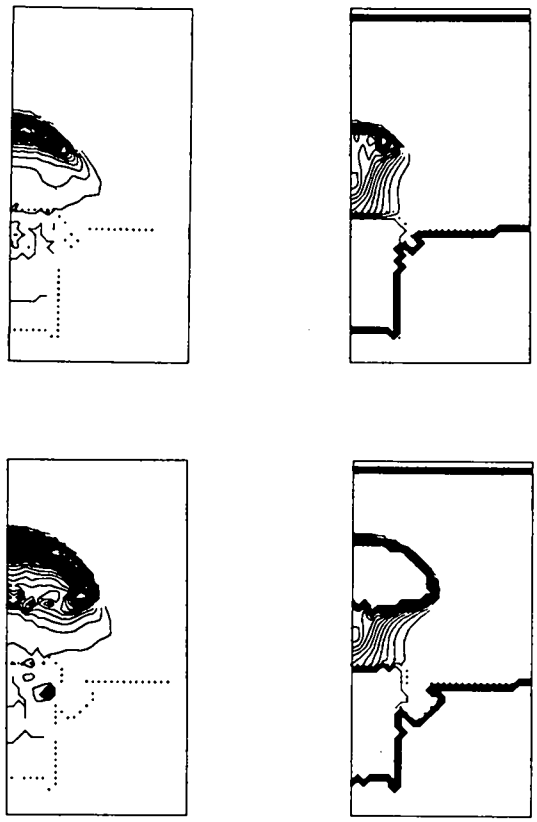

Fig. 8. Isobars (left) and contours of constant mass fraction at 1.91 μs (top) and 2.38 μs after impact by 7.62-mm cylinder at 873 m/s.

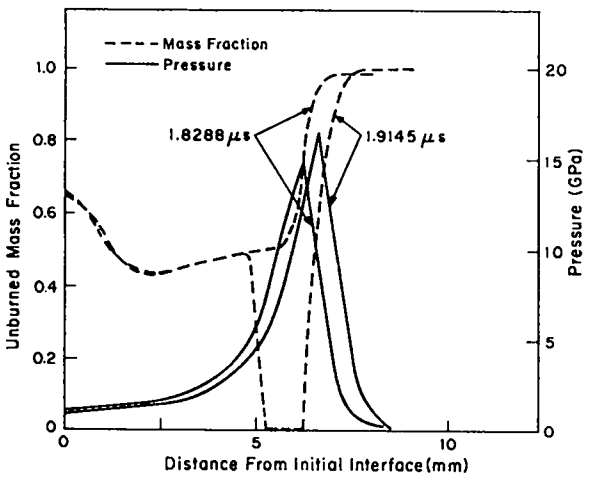

Fig. 9. Pressure and unburned mass fraction for 7.62-mm-diam cylinder impact at 873 m/s.

detonation builds up behind it. Eventually, a steady detonation wave will be reached with peak pressure equal to 33.5 GPa, slightly less than that of the Chapman-Jouguet point.

C. Cylinder, 3.35-mm-diam

Much higher velocities were required to cause a detonation in the experiments with the smaller cylinder. The same computational model was used, except that the mesh size was reduced to help resolve parameters on the smaller scale. The behavior of the explosive is quite different from that described previously for the larger cylinder. Figure 10 shows the peak pressure in the explosive plotted as a function of time after the impact for three different sets of conditions.

1. Impact at 2.093 km/s with the chemical reaction in the explosive turned off.
2. Impact at 2.093 km/s with the Forest Fire burn model (reaction turned on).
3. Impact at 2.178 km/s with the Forest Fire burn model.

In the first case, the peak pressure does not equal the 18.4 GPa predicted from matched Hugoniots for the nonreacted HE and steel. In

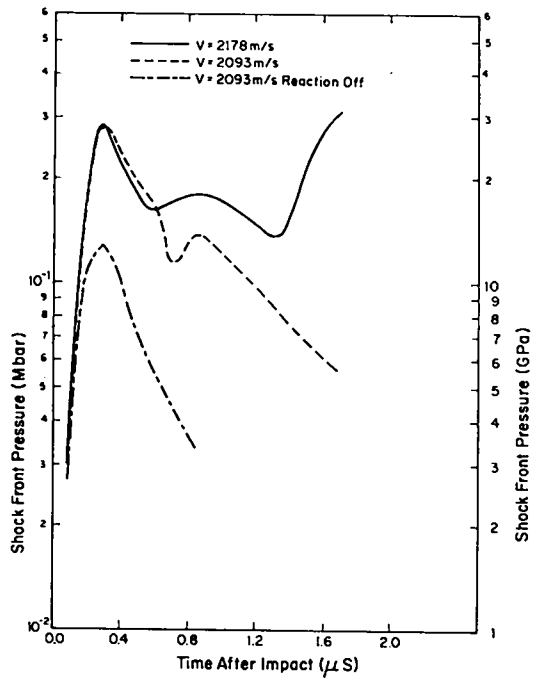

Fig. 10. Shock front pressure versus time for impact by 3.35-mm-diam cylinder.

the second case, the pressure rises in about 0.3 μs to about 28 GPa because of the reaction, but again falls off. Some of the computational cells near the centerline and the impact interface are completely reacted, a condition that ordinarily (in one-dimensional computations or in those just described for the larger cylinder) would propagate into a high-order detonation. Here the projectile is small enough that side rarefactions quickly reduce the peak pressure and the explosive does not detonate; this agrees with experimental observations. As a matter of interest, the failure diameter for PBX 9404 is 1.20 ± 0.2 mm, about 35% of the projectile's diameter. The failure diameter for PBX 9501 has not been determined, but should be approximately the same. In the third case, the peak pressure rises to about 28 GPa in the first 0.3 μs and falls to about 14 GPa about 1.0 μs after that. However, because the energy released in the chemical reaction is enough to overcome the effect of the side rarefactions, the peak pressure increases again and a full detonation results.

The isobars and contours of constant mass fraction for the latter two cases are compared in Fig. 11.

D. Sphere, 6.35-mm diam

The impact of the steel sphere with the PBX 9501 was calculated for one velocity, 1852 m/s. Recall that the experiments determined that no detonation occurred for seven tests with impact velocities ranging from 1.238 to 2.506 km/s. The isobars at 0.20 and 1.58 μs after impact are shown in Fig. 12. The effect of rarefactions can be seen at the sphere-HE interface. The peak pressure reached in this case is only 11 GPa versus 15.4 GPa that is predicted from matched Hugoniots for nonreacting explosive and steel.

V. COMPARISON WITH PREVIOUS RESULTS

Three similar studies of projectile impact on HE have recently been completed.[4-6] The

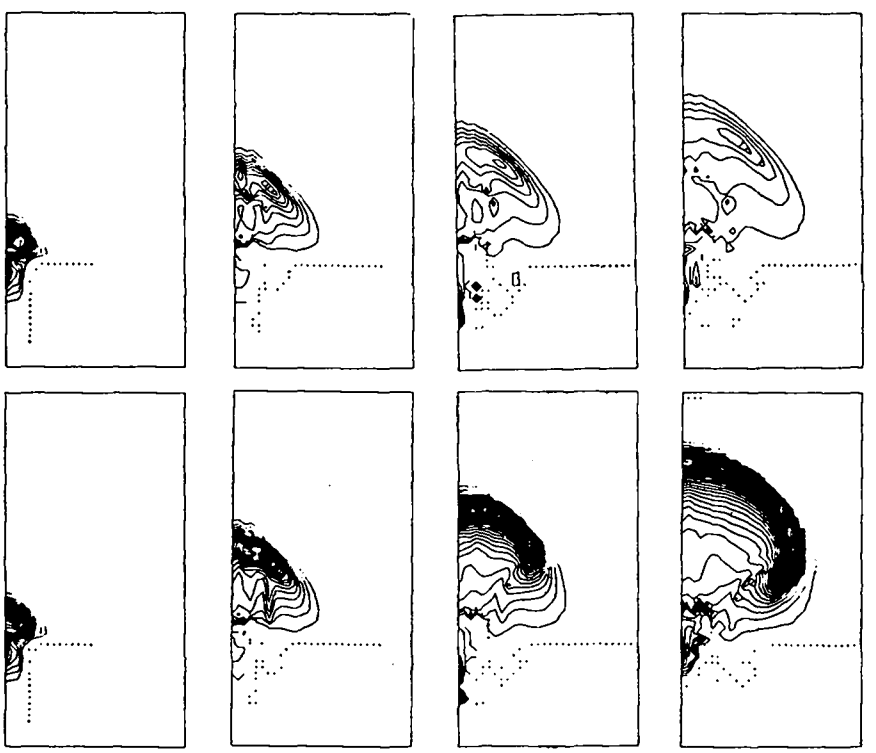

Fig. 11a. Isobars following impact of 3.35-mm-diam cylinder at 2093 m/s, at top and 2178 m/s, at bottom at 0.42, 1.26, 1.68, and 2.1 μs.

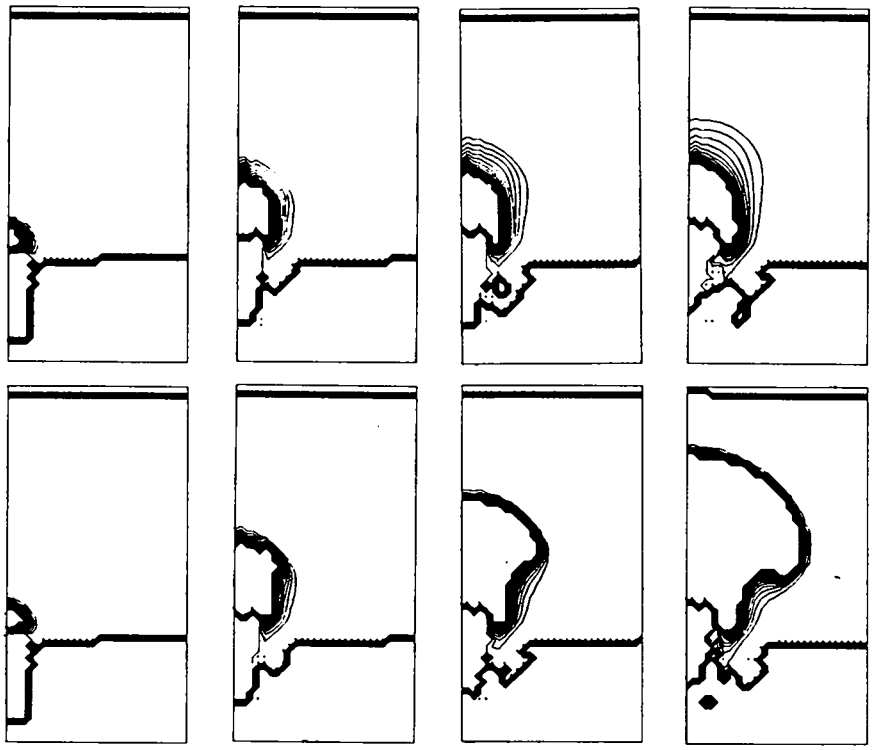

Fig. 11b. Contours of constant mass fraction following impact of 3.30-mm-diam cylinder at 2093 m/s, at top and 2178 m/s, at bottom at 0.42, 1.26, 1.68, and 2.1 μs.

study in Ref. 4 concentrated on PBX 9404 with impact by cylinders ranging from 1.27 to 20.32 mm in diameter. Some of the experiments included 2- and 6-mm tantalum sheets between the HE and the projectile. The data for the impact on bare HE are presented in Fig. 13 for comparison with the

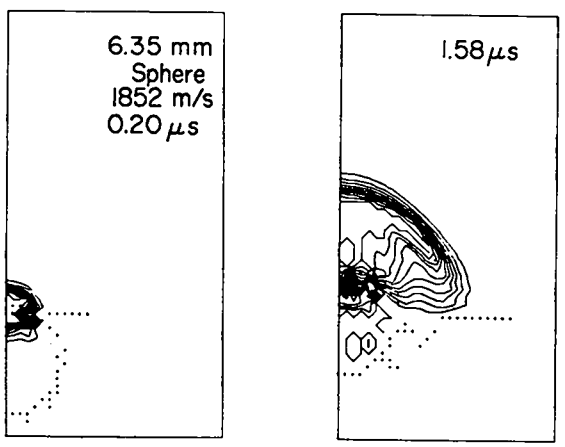

Fig. 12. Isobars at 0.20 μs and 1.58 μs after impact with 6.35-mm-diam sphere at 1852 m/s.

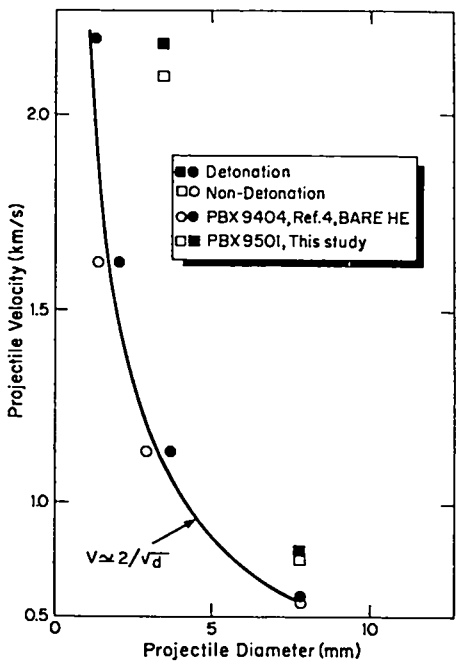

Fig. 13. Comparison with experimental data of Ref. 4.

results of this study. The PBX 9501 HE is less sensitive, as indicated by Fig. 7. Both Refs. 4 and 5 developed and applied simplified empirical models to predict the critical velocity for projectiles. Several models, discussed in Ref. 5, imply that the critical velocity for shock initiation varies inversely as the square root of the diameter. The data from Ref. 4 seem to fit this velocity dependence well, but the two data points from this study do not. Additional data points at intermediate diameters would be necessary to determine the true shape of the velocity-diameter dependence for PBX 9501.

VI. CONCLUSIONS

The shock-induced detonation of small samples of PBX 9501 by the impact of projectiles of different shapes and sizes has been modeled successfully. The results of the calculations are in good agreement with experimental observations. From considerations of projectile velocity, size, shape, and explosive properties, shock-induced detonations can be calculated for a range of parameters.

The curvature of the impact-induced shock wave caused by side rarefactions and geometric divergence is the major difference between this class of shock-induced detonation and that caused by a plane-wave lens or flyer plate. These effects cannot be scaled easily because of nonlinear interactions.

ACKNOWLEDGMENTS

This work was supported by the US Department of Energy, Office of Military Applications. We gratefully acknowledge the assistance and contributions of C. L. Mader, C. A. Forest, A. L. Bowman, J. D. Kershner, L. A. Gritzo, and L. W. Hantel. The instrumented projectile impact experiments were performed by G. H. Carlson, T. R. King, R. J. DeWitt, J. A. Sanchez, and K. C. Pederson; the uninstrumented experiments were performed by J. A. Sanchez and K. C. Pederson.

REFERENCES

1. C. L. Mader and C. A. Forest, "Two-Dimensional Homogeneous and Heterogeneous Detonation Wave Propagation," Los Alamos National Laboratory report LA-6259 (1976).
2. C. L. Mader, Numerical Modeling of Detonations (University of California Press, Berkeley, 1979).
3. J. D. Kershner and C. L. Mader, "2DE, A Two-Dimensional Continuous Eulerian Hydrodynamic Code for Computing Multicomponent Reactive Hydrodynamic Problems," Los Alamos National Laboratory report LA-4846 (March 1972).
4. H. C. Vantine (Compiler), "Shock Initiation of Bare- and Covered-PBX 9404 Charges by Projectile Impact," Lawrence Livermore National Laboratory report UCID-18547 (January 1980).
5. R. Frey, P. Howe, J. Trimble, and G. Melani, "Initiation of Explosive Charges by Projectile Impact," US Army Armament Research and Development Command, Aberdeen, Maryland, ARBRL-TR-02176 (June 1979).
6. C. L. Mader and G. H. Pimbley, "Jet Initiation of Explosives," Los Alamos National Laboratory report LA-8647 (1981).

APPENDIX A
EQUATION OF STATE

The HOM equation of state is used to solve for pressure P and temperature T in a cell, with specific volume V and specific internal energy I as input. The shock velocity U_s and the particle velocity U_p are related by

$$U_s = C + SU_p.$$

The equations for a solid are

$$P_H = C^2(V_o - V)/[V_o - S(V_o - V)]^2,$$

$$X = \ell n\ V,$$

$$\ell n\ T_H = F + GX + HX^2 + IX^3 + JX^4,$$

$$I_H = (1/2)\, P_H(V_o - V),$$

$$P = (\gamma/V)\ (I - I_H) + P_H, \text{ and}$$

$$T = (I - I_H)\ (23\ 890)/C_v + T_H.$$

The equations for a gas are

$$X = \ell n\ V,$$

$$Y = \ell n\ P_i,$$

$$Y = A + BX + CX^2 + DX^3 + EX^4,$$

$$\ell n\ I_i = K + LY + MY^2 + NY^3 + OY^4,$$

$$I_i = I_i - Z,$$

$$\ell n\ T_i = Q + RX\ \ SX^2 + TX^3 + UX^4,$$

$$-1/\beta = R + 2SX + 3TX^2\ 4UX^3,$$

$$P = [1/(\beta V)]\ (I - I_i) + P_i, \text{ and}$$

$$T = (I - I_i)\ (23\ 890)/C_v + T_i.$$

The solution for a cell with more than one component is based on combinations of these equations.[2,3]

The equation-of-state parameters used in this study are tabulated in Table A-I. The units are volume (cm^3/g), energy ($Mbar\text{-}cm^3/g$), pressure (Mbar), temperature (K), velocity (cm/μs), and heat capacity (cal/g-K).

TABLE A-I

EQUATION-OF-STATE PARAMETERS

PBX 9501

C	2.500000000000E-01	D	3.043215493500E-02
S	2.180000000000E+00	E	-1.632653561600E-02
F	-1.736298901400E+01	K	-1.612213734400E+00
G	-1.111079475900E+02	L	5.275117547200E-01
H	-1.941853902200E+02	M	7.024394327500E-02
I	-1.418535926800E+02	N	4.643524952000E-03
J	-3.359704507400E+01	O	1.234139635400E-04
γ	1.500000000000E+00	Q	7.366260658300E+00
C_v	3.000000000000E-01	R	-5.086700168300E-01
V	5.455537370400E-01	S	3.553568750600E-02
α	1.000000000000E-04	T	3.942242944100E-02
A	-3.525872840600E+00	U	-1.367380827300E-02
B	-2.602094152600E+00	C_v'	5.000000000000E-01
C'	2.615657058600E-01	Z	1.000000000000E-01

Steel

C	4.580000000000E-01	J	-1.663916159830E+03
S	1.510000000000E+00	γ	2.000000000000E+00
F	-3.823825874530E+03	C_v	1.070000000000E-01
G	-7.032119540240E+03	V	1.263104711000E-01
H	-4.826702138900E+03	α	1.170000000000E-05
I	-1.466784021180E+03		

Air

A	-4.506025426880E+00	O	-1.585218953380E-06
B	-1.275461106280E+00	Q	8.226445814410E+00
C'	-3.742766002920E-03	R	-2.515251309500E-01
D	1.239292367470E-02	S	-1.344469400470E-02
E	-2.076941229290E-03	T	1.408710164220E-02
K	-1.626554474380E+00	U	-2.181321899850E-03
L	9.052831466180E-02	C_v'	5.000000000000E-01
M	2.690049977260E-03	Z	1.000000000000E-01
N	-5.435831221920E-05	V	8.652240000000E+02

APPENDIX B
FOREST FIRE BURN RATE

The mass fraction of unburned explosive W is defined as W = 1 for pure solid, and burns to gaseous products, W = 0, according to a pressure-dependent rate law based on experimental data.[1,2] The rate R is defined for pressure P in Mbars and time t in μs by

$$R = (1/W)\ (dW/dt), \text{ and}$$

$$\ell n\ R = \sum_{i=1}^{N} C_i P^{i-1} .$$

The limiting conditions set R = 0 for P less than a specified cutoff pressure, and R = ∞ (W → 0 immediately) when P reaches the C-J pressure. The rate parameters used in this study are tabulated in Table B-I.

These Forest Fire parameters are derived from the experimentally determined Pop plots. The equation of the Pop plot is

$$\ell n\ x = A + B\ \ell n\ P,$$

with the run distance x in cm and the pressure P in Mbars. The Pop plots are shown in Fig. 1. The parameters are given in Table B-II.

TABLE B-I
FOREST FIRE RATE PARAMETERS
PBX 9501

C-J PRESSURE = 0.3595 CUT-OFF PRESSURE = 0.005

C(I=1,14) =

-9.8934158860E+00	5.0650030181E+02	-1.8667411206E+04
5.0905952790E+05	-9.4510392786E+06	1.2276466725E+08
-1.1353446359E+09	7.5536596868E+09	-3.6199460533E+10
1.2371591489E+11	-2.9390384021E+11	4.6087898934E+11
-4.2871378222E+11	1.7909975086E+11	

TABLE B-II
POP-PLOT PARAMETERS
PBX 9501

A	B
-5.082788910	-1.475248725

Printed in the United States of America
Available from
National Technical Information Service
US Department of Commerce
5285 Port Royal Road
Springfield, VA 22161

Microfiche $3.50 (A01)

Page Range	Domestic Price	NTIS Price Code	Page Range	Domestic Price	NTIS Price Code	Page Range	Domestic Price	NTIS Price Code	Page Range	Domestic Price	NTIS Price Code
001-025	$ 5.00	A02	151-175	$11.00	A08	301-325	$17.00	A14	451-475	$23.00	A20
026-050	6.00	A03	176-200	12.00	A09	326-350	18.00	A15	476-500	24.00	A21
051-075	7.00	A04	201-225	13.00	A10	351-375	19.00	A16	501-525	25.00	A22
076-100	8.00	A05	226-250	14.00	A11	376-400	20.00	A17	526-550	26.00	A23
101-125	9.00	A06	251-275	15.00	A12	401-425	21.00	A18	551-575	27.00	A24
126-150	10.00	A07	276-300	16.00	A13	426-450	22.00	A19	576-600	28.00	A25
									601-up	†	A99

†Add $1.00 for each additional 25-page increment or portion thereof from 601 pages up.